Pergamon

Int. J. Heat Mass Transfer. Vol. 39, No. 2, pp. 319–329, 1996

0017-9310/96 $9.50+0.00

0017-9310(95)00118-2

Convective heat transfer in porous and overlying fluid layers heated from below

SUNG JIN KIM
Thermal Engineering Center, IBM Storage Systems Division, Tucson, AZ 85744, U.S.A.

and

CHRISTOPHER Y. CHOI
Department of Agricultural and Biosystems Engineering, The University of Arizona, Tucson, AZ 85721, U.S.A.

(*Received* 8 *June* 1994 *and in final form* 10 *March* 1995)

Abstract—The onset of convection when a porous layer underlying a fluid layer is heated from below has been numerically investigated. In order to validate the interface boundary conditions along with the numerical scheme, the present study has focused on the critical Rayleigh number and the corresponding number of cells. In addition, the effects of the Rayleigh number, aspect ratio and thickness ratio on supercritical convection in the composite layer have been investigated. The results show that the number of cells at the critical Rayleigh number (Ra_{pc}) is in good agreement with the previous report based on the linear stability theory. The abrupt change in convective flow patterns accurately verifies the precipitous drop of Ra_{pc} with the increasing the depth ratio (d) and the rapid change of the wave number (a_p) near $d = 0.12$. As Ra_p increases, the cell size changes for all depth ratios ($d = 1.0$, 0.5, 0.2, 0.1 and 0). In particular, heat transfer rate changes dramatically due to the effects of the aspect ratio and the corresponding number of cells when $d = 0.1$.

1. INTRODUCTION

Thermal and chemical interaction between a saturated porous layer and an overlying fluid layer can be encountered in many engineering and environmental applications. A typical example of this configuration is the liquid alloys above the frozen alloys at the bottom, separated by a mushy zone, when the mold containing concentrated alloys is cooled from below for directional solidification. The mushy zone consisting of dendrites immersed in the melt can be modeled as a porous medium with variable permeability in theoretical and computational investigations. Another interesting application can be found in the accurate modeling of boundary conditions at the soil and water interface. Over the past decade, there has been increasing concern about soil and water contamination from industrial and agricultural chemicals. Therefore, an understanding of the transport phenomena from soil to water, and vice versa, and of the corresponding interface boundary conditions has become important. To model the interface boundary conditions and to confirm the accuracy, the energy equation instead of the chemical transport equation can be chosen because of the mathematical similarity of those equations. In addition, the study can also be applied to many other practical problems such as packed-bed thermal storage systems, fibrous granular insulation and porous journal bearing, to name a few. Prasad [1] reported an extensive review of this subject, and Nield and Bejan [2] devoted a section to it in their book on convection in porous media.

The onset of convection when a porous layer underlying a fluid layer is heated from below was first studied by Sun [3]. From a linear stability analysis, the critical Rayleigh number in the porous medium was found to decrease continuously as the thickness ratio of the fluid layer to the porous layer increases. Later Chen and Chen [4] found that Sun [3] had overlooked the bimodal nature of the marginal stability curve. Their results clearly showed two relative minima at low thickness ratio. They also found that there exists a critical thickness ratio at which the critical wavelength decreases by almost one order of magnitude. Later Chen and Chen [5] performed a series of experiments to verify their theoretical results. They observed that the porous-layer-dominated convection changes to the fluid-layer-dominated convection as the thickness ratio increases.

In an effort to obtain information for supercritical convection phenomena, Poulikakos [6] studied the same problem of flow instability in a horizontal composite layer bounded by four solid walls. Using a control-volume-based finite difference method, he observed significant flow penetration from the fluid layer into the porous layer for a Darcy number of 10^{-4}. His numerical investigation was based on the Darcy–Brinkman–Forchheimer equation for the

NOMENCLATURE

A	aspect ratio, H/L
a_p	wavenumber for the porous layer
c	specific heat
d	depth ratio, h_f/h_p
Da	Darcy number, K/H^2
F	Forchheimer number
g	gravity constant
H	total thickness of fluid and porous layers
h_f, h_p	thickness of fluid and porous layers
k	thermal conductivity
K	permeability
L	horizontal length of the calculation domain
n	number of iterations
N	number of cells
Nu	Nusselt number, equation (14c)
p	pressure
Pr	Prandtl number, ν/α_p
Ra	Rayleigh number for the fluid layer, $g\beta(T_0-T_t)h^3/\nu\alpha$
Ra_H	Rayleigh number based on H, $g\beta(T_b-T_t)H^3/\nu\alpha$
Ra_p	Rayleigh number for the porous layer, $g\beta(T_b-T_o)h_pK/\nu\alpha_{eff}$
S	source team
T	temperature
$\mathbf{v}$	velocity vector (u, v)
x, y	horizontal and vertical coordinates.

Greek symbols

α	thermal diffusivity of fluid
α_p	thermal diffusivity of porous medium
β	thermal expansion coefficient of fluid
ζ	vorticity
θ	dimensionless temperature
λ	wavelength
Λ_H	inertia parameter, $F\phi H/\sqrt{K}$
ν	kinematic viscosity
ρ	density
ϕ	porosity
ψ	stream function.

Subscripts

eff	effective thermophysical properties
f, p	fluid and porous layers
o	interface
t, b	top and bottom boundaries.

Superscripts

*	dimensionless parameters.

porous layer. In his study, the conductivity of the porous medium was always equal to that of the fluid. Recently, Chen and Chen [7] performed a numerical investigation of the same problem using a combined Galerkin and finite difference method. They varied the Rayleigh number of the porous layer up to 20 times the critical Rayleigh number. The horizontal extent of the computational domain for all supercritical Rayleigh numbers was fixed to one critical wavelength, which they had predicted earlier at onset by the linear stability theory. They imposed periodic conditions on the lateral boundaries. The Nusselt number for the thickness ratio less than the critical value was found to increase with the Rayleigh number of the porous layer, while the increase was rather moderate at a larger thickness ratio. Their numerically predicted Nusselt numbers agreed well with the experimental results. Prasad *et al.* [8] and Prasad and Tian [9] conducted a flow visualization study in a cylindrical cavity heated from below. They observed that the number of convective cells in the composite layer depends on the Rayleigh number, the Darcy number, the thickness ratio and the aspect ratio.

The purpose of the present investigation is, first, to understand the convective and diffusive phenomena between porous and overlying fluid layers. Second, the present calculations will focus on validating the accuracy of the interface boundary conditions along with the numerical scheme by extending the previous studies [4–7] from the onset of natural convection to supercritical Rayleigh number convection. Therefore, the critical Rayleigh numbers based on the linear stability theory will be numerically verified. In addition, the effects of the Rayleigh number, aspect ratio and thickness ratio on the fluid flow and heat transfer will be studied. The present investigation will provide a fundamental framework for predicting heat transfer, chemical diffusion and fluid flow between a fluid and a saturated porous medium.

2. FORMULATION

2.1. *Mathematical formulation*

The coordinate system and the corresponding physical configuration are shown in Fig. 1. The thickness of the fluid-saturated porous layer is h_p and the thickness of the fluid layer is h_f. The porous layer has

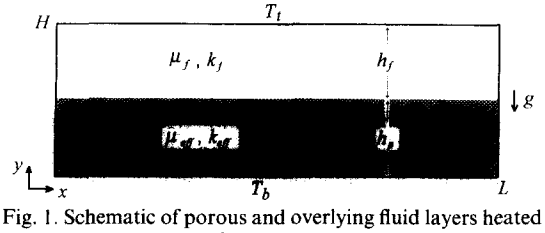

Fig. 1. Schematic of porous and overlying fluid layers heated from below.

viscosity μ_{eff} and thermal conductivity k_{eff}, while the overlying fluid layer has viscosity μ_f and thermal conductivity k_f. The bottom wall is maintained at constant temperature T_b and the upper wall is held at T_t. It is assumed that the flow is steady, laminar, incompressible and two-dimensional. In addition, the thermophysical properties of the fluid and the porous matrix are assumed to be constant, and the fluid-saturated porous medium is considered homogeneous and isotropic and in local thermodynamic equilibrium with the fluid. The conservation equations for mass, momentum and energy in the fluid region are

$$\nabla \cdot \mathbf{v} = 0 \tag{1}$$

$$\mathbf{v} \cdot \nabla \mathbf{v} = -\frac{1}{\rho_f}\nabla p + \nu_f \nabla^2 \mathbf{v} + g \tag{2}$$

$$\mathbf{v} \cdot \nabla T = \alpha_f \nabla^2 T. \tag{3}$$

The conservation equations for the porous region are based on a general flow model, which includes the effects of flow inertia as well as friction caused by macroscopic shear. This generalized flow model was semi-empirically derived and is known as the Brinkman–Forchheimer-extended Darcy model [10, 11]. The governing equations for the porous layer are

$$\nabla \cdot \mathbf{v} = 0 \tag{4}$$

$$\mathbf{v} \cdot \nabla \mathbf{v} = -\frac{1}{\rho_f}\nabla p + \nu_{\text{eff}} \nabla^2 \mathbf{v} - \frac{\nu_f}{K}\mathbf{v} - \frac{F}{\sqrt{K}}|\mathbf{v}|\mathbf{v} + g \tag{5}$$

$$\mathbf{v} \cdot \nabla T = \alpha_{\text{eff}} \nabla^2 T \tag{6}$$

where the effective thermal diffusivity α_{eff} is defined as $\alpha_{\text{eff}} = k_{\text{eff}}/(\rho_f c_f)$. The appropriate boundary conditions for the present problem are

$$u = 0 \quad v = 0 \quad T = T_b \quad \text{at} \quad y = 0 \tag{7a}$$

$$u = 0 \quad v = 0 \quad T = T_t \quad \text{at} \quad y = H \tag{7b}$$

$$u = 0 \quad v = 0 \quad \frac{\partial T}{\partial x} = 0 \quad \text{at} \quad x = 0 \quad \text{and} \quad L. \tag{7c}$$

In addition, the following matching conditions have to be satisfied at the interface of the porous/fluid layer:

$$u|_{y=h_p^-} = u|_{y=h_p^+} \quad v|_{y=h_p^-} = v|_{y=h_p^+} \tag{8a}$$

$$p|_{y=h_p^-} = p|_{y=h_p^+} \tag{8b}$$

$$\mu_{\text{eff}}\left(\frac{\partial u}{\partial y} + \frac{\partial v}{\partial x}\right)\bigg|_{y=h_p^-} = \mu_f\left(\frac{\partial u}{\partial y} + \frac{\partial v}{\partial x}\right)\bigg|_{y=h_p^+} \tag{8c}$$

$$T|_{y=h_p^-} = T|_{y=h_p^+} \quad k_{\text{eff}}\frac{\partial T}{\partial y}\bigg|_{y=h_p^-} = k_f\frac{\partial T}{\partial y}\bigg|_{y=h_p^+}. \tag{8d}$$

These conditions express the continuity of longitudinal and transverse velocities, pressure, deviatoric normal and shear stresses, temperature and the heat flux. Equation (8b) implies the matching condition of the total normal stress at the interface. The condition in equation (8c) represents the matching shear stress, which is an extension of the condition used by Neale and Nader [12] and Vafai and Kim [13] for flow that is not parallel to the porous/fluid interface. Some controversy still exists over which boundary conditions should be used at the interface. Some investigators prefer to use Beavers and Joseph's slip velocity condition at the interface with the Darcy flow model. Others prefer boundary conditions [equations (8a)–(8d)] with the general flow model because it enables them to incorporate the single domain approach. Kaviany [11] presented a thorough review on the slip coefficient, which depends on the interfacial location, the particle Reynolds number, the gap size, the permeability, the porosity, the surface structure of the porous medium, etc. In this paper the single-domain approach, which will be explained later, was adopted in order to examine its accuracy. This is also effective for studying the motion of the fluid in the region which is partially filled with a porous medium and partially filled with a regular fluid. The effective viscosity in the porous medium can be approximated to be equal to the fluid viscosity as in Neale and Nader [12]. In addition, the effect of the thermal dispersion in the porous matrix is assumed to be constant and is incorporated in the effective thermal conductivity for simplicity in the presentation of the results.

2.2. *Numerical simulation*

In modeling a composite fluid and porous system, one can use the two-domain approach where fluid and porous layers are treated separately with coupling conditions at the interface. This approach, however, would require an involved iterative procedure for matching the interface conditions. A more efficient alternative is to use the continuum approach where two sets of equations for the fluid and the porous regions are combined into one set of conservation equations [14]. In other words, both the porous and the fluid layers can be modeled as a single domain governed by one set of equations, the solution of which satisfies the continuity of the velocity, stress, temperature and the heat flux across the porous/fluid interface as described in equations (8a)–(8d).

By introducing the stream function and the vorticity as

$$u = \frac{\partial \psi}{\partial y} \quad v = -\frac{\partial \psi}{\partial x}$$

$$\zeta = \frac{\partial v}{\partial x} - \frac{\partial u}{\partial y}$$

equations (4)–(6) become the dimensionless vorticity transport equation, stream function equation and energy equation, respectively. These equations are valid throughout the composite layer.

$$\frac{\partial \psi^*}{\partial y^*}\frac{\partial \zeta^*}{\partial x^*} - \frac{\partial \psi^*}{\partial x^*}\frac{\partial \zeta^*}{\partial y^*} = Pr\,\nabla^2 \zeta^* + Pr\,Ra_H \frac{\partial \theta}{\partial x^*} + S^* \tag{9}$$

$$\nabla^2\psi^* = -\zeta^* \tag{10}$$

$$\frac{\partial\psi^*}{\partial y^*}\frac{\partial\theta^*}{\partial x^*} - \frac{\partial\psi^*}{\partial x^*}\frac{\partial\theta^*}{\partial y^*} = \nabla\cdot\left(\frac{k}{k_f}\nabla\theta\right) \tag{11}$$

where in the fluid layer

$$S^* = 0 \qquad k = k_f \tag{12a}$$

and in the porous layer

$$S^* = -\frac{Pr}{Da_H}\zeta^* - \Lambda_H\sqrt{[(u^*)^2+(v^*)^2]}\zeta^* \qquad k = k_{eff}. \tag{12b}$$

Note that all the variables have been non-dimensionalized based on the following definitions:

$$x^* = \frac{x}{H} \quad y^* = \frac{y}{H} \quad u^* = \frac{Hu}{\alpha_f} \quad v^* = \frac{Hv}{\alpha_f}$$

$$\psi^* = \frac{\psi}{\alpha_f} \quad \zeta^* = \frac{H^2\zeta}{\alpha_f} \quad \theta = \frac{T-T_t}{T_b-T_t}.$$

The dimensionless boundary conditions are

$$u^* = 0 \quad v^* = 0 \quad \theta = 1 \quad \text{at} \quad y^* = 0 \tag{13a}$$

$$u^* = 0 \quad v^* = 0 \quad \theta = 0 \quad \text{at} \quad y^* = 1 \tag{13b}$$

$$u^* = 0 \quad v^* = 0 \quad \frac{\partial\theta}{\partial x} = 0 \quad \text{at} \quad x^* = 0 \quad \text{and} \quad L/H. \tag{13c}$$

A control-volume-based finite difference method was employed to solve the system of partial differential equations for the vorticity, stream function and temperature [15]. The control-volume formulation has an attractive feature, i.e. the resulting solution would imply that the integral conservation of mass, momentum and energy is satisfied over the entire domain as well as any group of control volumes. The harmonic mean formulation was used to handle abrupt variations in the thermophysical properties, such as the permeability and thermal conductivity, across the interface. This ensured the continuity of convective and diffusive fluxes across the interface without requiring the use of an excessively fine grid structure.

The finite difference equations were solved by the extrapolated Jacobi scheme. This iterative scheme is based on a double cyclic routine, which translates into a sweep of only half of the grid points at each iteration step [16]. The present FORTRAN program was vectorized so that it was used efficiently when processed on a Convex 240 mini-supercomputer. It was also necessary to use underrelaxation to ensure convergence.

Small perturbations may be included as part of the initial conditions, and stability and instability may be differentiated by the decay or growth of the perturbations. In the present study, however, the propagation of the bottom boundary condition naturally caused the initial disturbance after a few iterations. Such a disturbance would either trigger the instability or be suppressed depending upon the Rayleigh number.

Additional calculations were carried out in order to evaluate the effects of the porous material on the heat transfer rate at the horizontal bounding walls. The results for the heat transfer rate were represented in a dimensionless form of the Nusselt number, i.e. at the lower wall the Nusselt number can be expressed as

$$Nu_b = \frac{Q}{k_{eff}(L/h_p)(T_t - T|_{y=h_p})} = \left(\frac{k_f}{k_{eff}} + \frac{h_f}{h_p}\right)\frac{h_p}{L}\int_0^{L/H}\left.\frac{\partial\theta}{\partial x^*}\right|_{y^*=0} dx^* \tag{14a}$$

and at the upper wall

$$Nu_t = \frac{Q}{k_f(L/h_f)(T|_{y=h_p} - T_t)} = \left(\frac{k_f}{k_{eff}} + \frac{h_f}{h_p}\right)\frac{h_p}{L}\int_0^{L/H}\left.\frac{\partial\theta}{\partial x^*}\right|_{y^*=1} dx^* \tag{14b}$$

and therefore, the overall averaged Nusselt number is

$$Nu = \frac{Nu_t + Nu_b}{2}. \tag{14c}$$

Note that these Nusselt numbers are unity when the heat is transferred only by conduction. Also the Nusselt number results are proportional to the overall heat flux through the bottom and the top walls, and therefore they were used as an additional check to ensure the overall energy balance. The difference between Nu_b and Nu_t was within 1% for the present study.

2.3. *Stability and accuracy of the numerical scheme*

The numerical integration was performed until the following convergence criterion was satisfied:

$$\max\left|\frac{\varphi_{i,j}^{n+1} - \varphi_{i,j}^n}{\varphi_{i,j}^n}\right| < 10^{-6} \tag{15}$$

where φ stands for ζ^*, ψ^* and θ, and n denotes the iteration number. The stability of the numerical scheme was found to be somewhat insensitive to the choice of grid size. We employed a proper combination of Δx and Δy to assure stability. This was done by a systematic decrease in the grid size until further refinement of the grid size showed no more than 1% difference in the convergent results. The physical domain was covered by a non-uniform rectangular grid system consisting of m horizontal and n vertical lines. After extensive test runs, either 82×82 or 164×82 non-uniform grids were chosen and used depending upon the depth ratio and the corresponding aspect ratio. In particular, the grid size was carefully selected in order to obtain an accurate number of the recirculation cells for each case. Calculations were made for the parameters used by Chen and Chen [7] for the purpose of comparison, i.e. ϕ (porosity) = 0.389, $Da_p = K/h_p^2 = 0.8897\times10^{-5}$ and $k_f/k_p = 0.725$.

3. RESULTS AND DISCUSSION

To qualify the present numerical code, two sets of numerical results were obtained for the well-known Bénard convection problem. First, with the fluid layer only, the present numerical code slightly underpredicts the Nusselt number compared with Silverton's experimental data [17] as shown in Fig. 2(a). The critical Rayleigh number is found to be approximately 1780, while the value is 1708 from the linear stability analysis. The delay of the onset of the natural convection is due to the influence of the lateral walls on the convective process. As Catton [18, 19] indicated, lateral walls introduce additional viscous shear, which delays the onset of motion in a fluid layer. The regression line based on the present numerical data is slightly upwardly convex, and such a trend is reasonable considering the additional empirical data points at higher Ra. On the other hand, Fig. 2(b) shows that the critical Rayleigh number for the porous medium is approximately 40, which is quite close to the $4\pi^2$ determined by the linear stability theory. When Ra_p increases in the supercritical range, the Nusselt numbers determined by the present numerical code are close to the regression lines by Elder and by Buretta and Berman (summarized in ref. [20]). When the aspect ratio is four, an abrupt change of the slope in Nu is observed as Ra_p increases from 60 to 70. Such a trend is mainly due to the restructuring of the recirculating cells within the limited space, and the number of cells is continuously increasing as Ra_p increases. As expected, the change of the slope has been rather smoothed when the aspect ratio is doubled. Poulikakos [21] also reported the significant effects of aspect ratio on maximum temperature in a heat-generating porous cavity largely due to the varying number of cells.

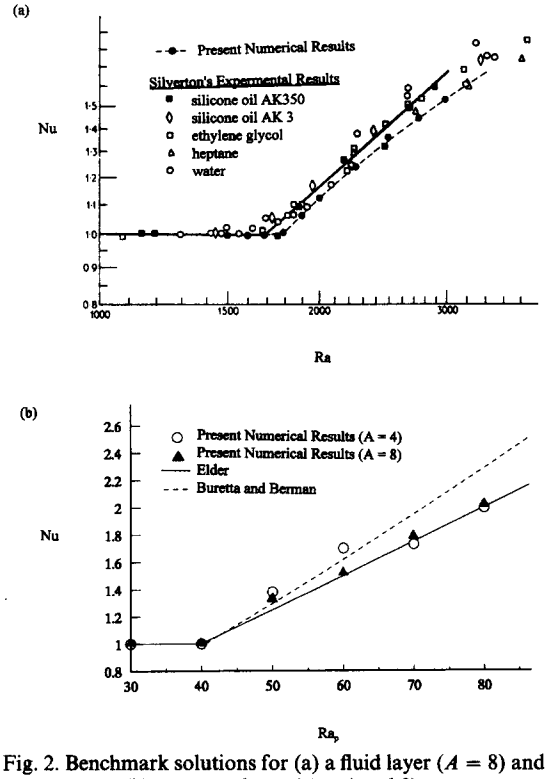

Fig. 2. Benchmark solutions for (a) a fluid layer ($A = 8$) and (b) a porous layer ($A = 4$ and 8).

In an effort to simulate convective phenomena and compare with the previous results [4] without restricting the size of cells, a different aspect ratio ($A = H/L$) was chosen for each depth ratio ($d = h_f/h_p$) with careful consideration of the expected cell size based on the linear stability [4, 7]. For $d = 1$, the aspect ratio is chosen as 5. For $Ra_p < Ra_{pc}$, the Nusselt number is unity, which indicates that the heat transfer is due solely to conduction. At $Ra_p = Ra_{pc}$, the Nusselt number remains unity, and as shown in Fig. 3(g), the horizontal isotherms indicate that no fluid motion has yet occurred. However, the initial formation of nine recirculating cells is shown in Fig. 3(a), although the streamlines are physically meaningless (i.e. the dimensional velocities based on ψ are so small as to be negligible). It should be noted that the calculations at and near the onset point require an excessive number of iterations. Consequently, extreme care was taken to ensure that the further iteration would not change the present results. The total number of the cells (N) can be transformed to the wavenumber (a_p) as

$$a_p = \frac{2\pi}{\lambda} = \frac{\pi N}{A(1+d)} \tag{16}$$

where λ indicates the wavelength. For $d = 1$ and $A = 5$, therefore, the wavenumber becomes 2.83 compared with 2.86 calculated by the linear stability theory [7]. When $Ra_p = 1.1Ra_{pc}$, as shown in Fig. 3(b) and (h), the isotherms are slightly wavy in the fluid region because of the weak fluid motion after the onset of natural convection. As Ra_p/Ra_{pc} increases to 1.5 and higher, the number of cells increases continuously, and the corresponding isotherms show active natural convection. Figures 3(f) and (l) show 16 cells and vigorous thermal plumes due to strong natural convection at $Ra_p/Ra_{pc} = 20$. It is interesting to observe that even the streamlines at $Ra_p/Ra_{pc} = 20$ do not penetrate the porous layer, and consequently the heat transfer mode is conduction in that region.

As mentioned earlier, Chen and Chen [7] performed numerical calculations with the computational domain equal to the critical wavelength for all supercritical cases. Their results showed that the changes in Nu were reasonably small at various a_p and justified the use of the cell size based on the critical wavenumber. With the present numerical scheme, the results for a_p and Nu were obtained and compared with the previous data. Figure 4 shows that the wavenumber, and thus the number of cells, increases as Ra_p increases. The present results somewhat underestimate Nu, and the assumption made by Chen and Chen [7] was in fact reasonable for this particular depth ratio ($d = 1$).

Further calculations for $d = 0.5$ and 0.2 reveal that the present numerical scheme accurately predicts the

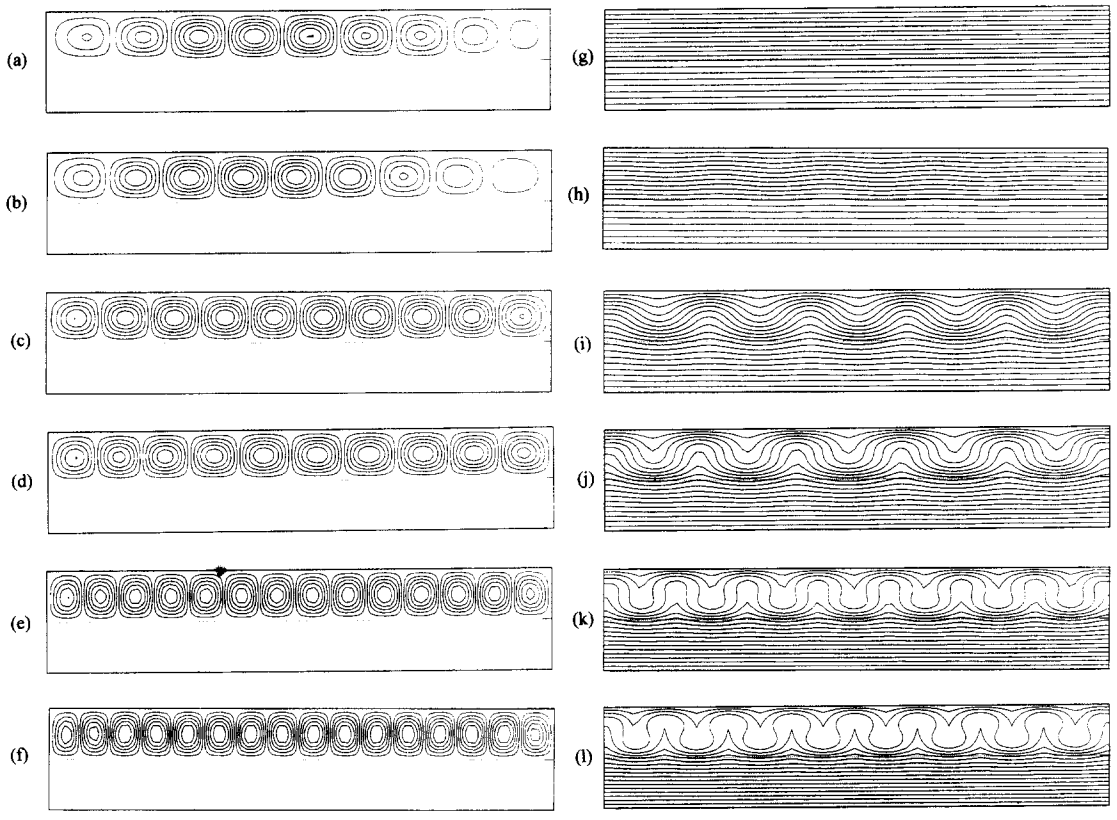

Fig. 3. Streamlines (left) and isotherms (right) for $d = 1.0$ ($\Delta\theta = 0.05$ for all cases): (a), (g) $Ra_p = Ra_{pc}$ ($\Delta\psi = 5.59 \times 10^{-5}$); (b), (h) $Ra_p = 1.1Ra_{pc}$($\Delta\psi = 4.82 \times 10^{-2}$); (c), (i) $Ra_p = 1.5Ra_{pc}$ ($\Delta\psi = 3.53 \times 10^{-1}$); (d), (j) $Ra_p = 3Ra_{pc}$ ($\Delta\psi = 7.88 \times 10^{-1}$); (e), (k) $Ra_p = 10Ra_{pc}$ ($\Delta\psi = 1.38 \times 10^{0}$); (f), (l) $Ra_p = 20Ra_{pc}$ ($\Delta\psi = 1.72 \times 10^{0}$).

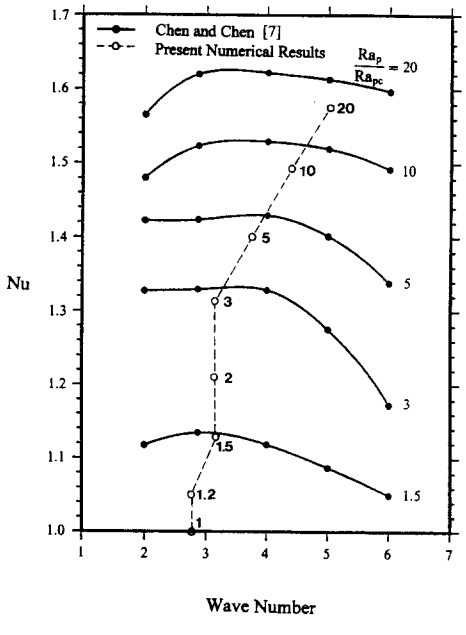

Fig. 4. Variation of the Nusselt number and the wavenumber with Ra_p/Ra_{mc} when $d = 1.0$.

number of recirculating cells at the onset point. The aspect ratios were selected as 5 and 2 for $d = 0.5$ and 0.2, respectively. Figure 5(a) shows, for example, that the number of cells is 10 for $d = 0.2$, and the corresponding wavenumber, 13.09, is compared with the curve fit based on the linear stability theory in Fig. 6. Again, the increase in Ra_p consistently produces additional cells, and the convective heat transfer mode is restricted in the fluid layer as depicted in Figs. 5(b), (c), (e) and (f). For $d = 0.5$, the wavenumber from the present calculations is overpredicted by about 2.9% in comparison with the curve fit in Fig. 6.

Sun [3] first studied the onset of the thermal convection in a composite layer system. However, he overlooked the bimodal nature of the marginal stability curve when $d < 0.15$, and later Chen and Chen [4] corrected his results. In particular, they uncovered the precipitous drop of the critical Ra_p and the rapid change of the critical wavenumber near $d = 0.12$ as shown in Fig. 6. The reason for such an abrupt change in the size of recirculating cells is that the convection pattern is dominated by the fluid layer for $d > 0.12$, while the convection pattern is dominated by the porous layer for $d < 0.12$ with the cell size determined

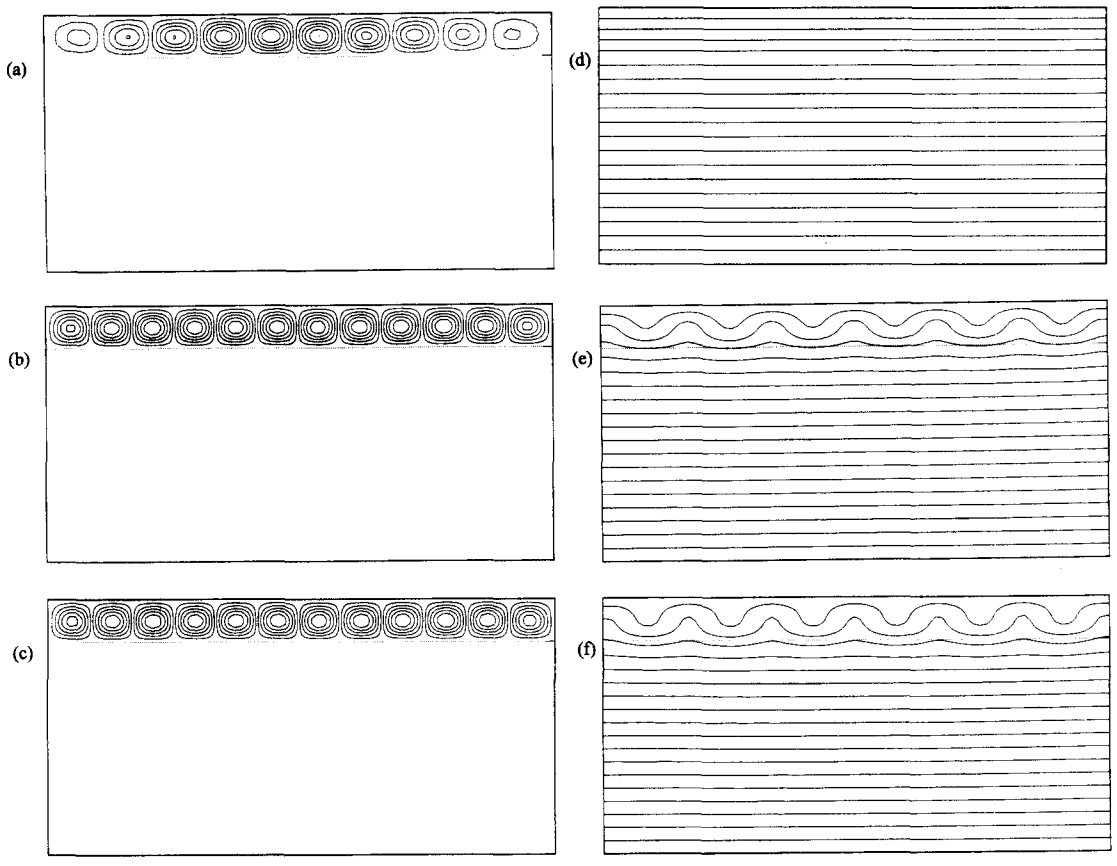

Fig. 5. Streamlines (left) and isotherms (right) for $d = 0.2$ ($\Delta\theta = 0.05$ for all cases): (a), (d) $Ra_p = Ra_{pc}$ ($\Delta\psi = 1.69 \times 10^{-5}$); (b), (e) $Ra_p = 2Ra_{pc}$ ($\Delta\psi = 4.39 \times 10^{-1}$); (c), (i) $Ra_p = 3Ra_{pc}$ ($\Delta\psi = 6.51 \times 10^{-1}$).

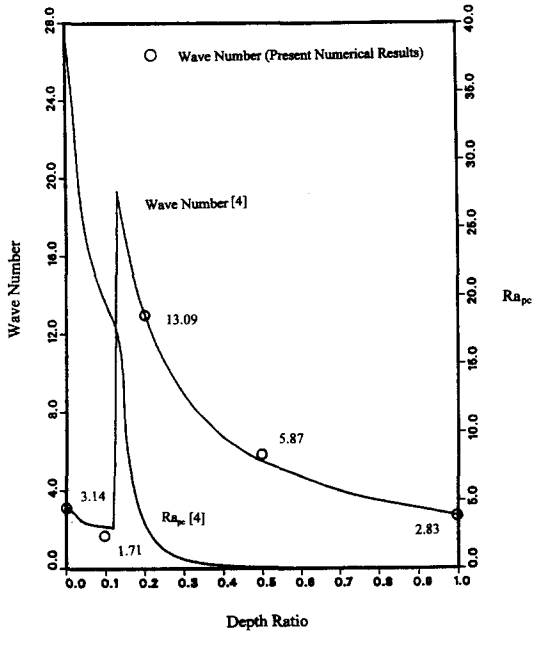

Fig. 6. Variation of the critical Nusselt number and the wavenumber with the depth ratio.

by the porous layer depth. Consequently, the wavenumber changes almost tenfold at $d = 0.12$. Later they extended the study with experiments [5], and further calculated the Nusselt number for $d = 0.1$ when $1 \leqslant Ra_p/Ra_{pc} \leqslant 20$ using a combined Galerkin and finite difference method with the restriction of the computational domain predetermined by the linear stability theory [7].

In the present investigation, we performed the calculations without restricting the computational domain. It should also be noted that 82 non-uniform grid points in the vertical direction were used based on careful numerical experiments, and the number of grid points is substantially less than the 550 grid points used by Chen and Chen [7] for $d = 0.1$. A few aspect ratios were tested, and $A = 10$ is selected for this depth ratio with 164 grid points in the horizontal direction for the present calculations. When $Ra_p/Ra_{pc} = 1$, an excessive number of iterations (50 000) were required to capture the initial formation of recirculating cells. Further iterations did not improve either the energy balance or the pattern of streamlines. The streamlines in Fig. 7(a) show the formation of six cells, and the corresponding isotherms in Fig. 8(a) indicate the con-

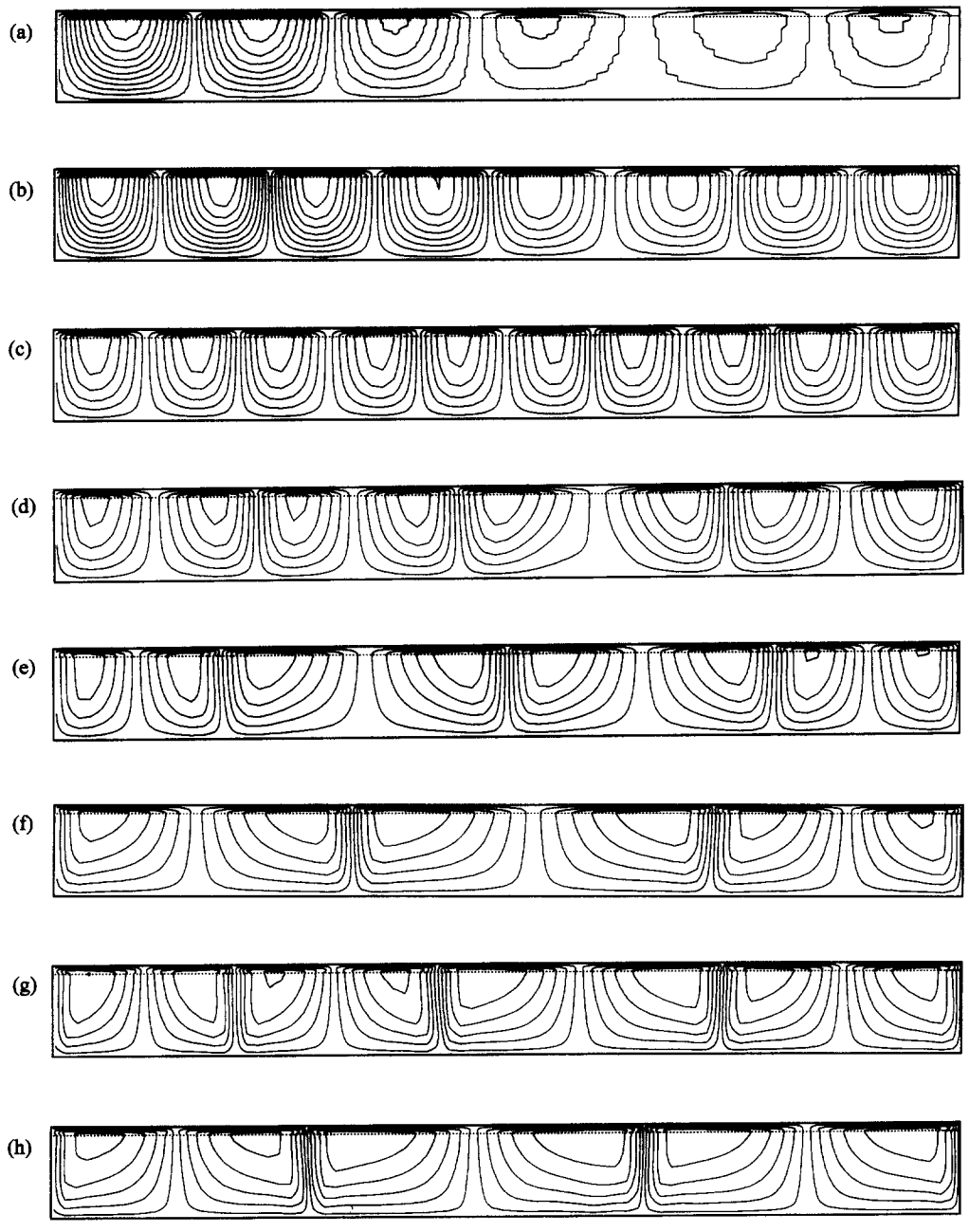

Fig. 7. Streamlines for $d = 0.1$: (a) $Ra_p = Ra_{pc}$ ($\Delta\psi = 5.95 \times 10^{-6}$); (b) $Ra_p = 1.5Ra_{pc}$ ($\Delta\psi = 3.85 \times 10^{-3}$); (c) $Ra_p = 2Ra_{pc}$ ($\Delta\psi = 8.17 \times 10^{-1}$); (d) $Ra_p = 3Ra_{pc}$ ($\Delta\psi = 1.46 \times 10^{0}$); (e) $Ra_p = 5Ra_{pc}$ ($\Delta\psi = 2.27 \times 10^{0}$); (f) $Ra_p = 10Ra_{pc}$ ($\Delta\psi = 3.93 \times 10^{0}$); (g) $Ra_p = 15Ra_{pc}$ ($\Delta\psi = 4.64 \times 10^{0}$); (h) $Ra_p = 20Ra_{pc}$ ($\Delta\psi = 5.91 \times 10^{0}$).

ductive heat transfer mode. The streamlines clearly demonstrate that the size of the recirculating cells is determined by the thickness of the porous layer, i.e. the natural convection is dominated by the porous layer. The corresponding wavenumber, 1.71, is somewhat less than the predicted value, 2.16, calculated by the linear stability theory because of the relatively limited space for the size of the recirculating cell in comparison with other calculated cases.

The subsequent calculations for $Ra_p/Ra_{pc} > 1$ initially exhibit the increase in the number of recirculating cells as shown in Figs. 7(b) and (c). Such a trend was previously observed when $d = 1$ and 0.2. As Ra_p/Ra_{pc} increases from 2 to 3, however, the number of cells unexpectedly decreases from 10 to eight as shown in Fig. 7(d) and remains the same at $Ra_p/Ra_{pc} = 5$. As Ra_p/Ra_{pc} increases to 10, the number of cells decreases further to six. Then the number is back to eight at $Ra_p/Ra_{pc} = 15$, and again decreases to six at $Ra_p/Ra_{pc} = 20$. It is interesting to find that the recir-

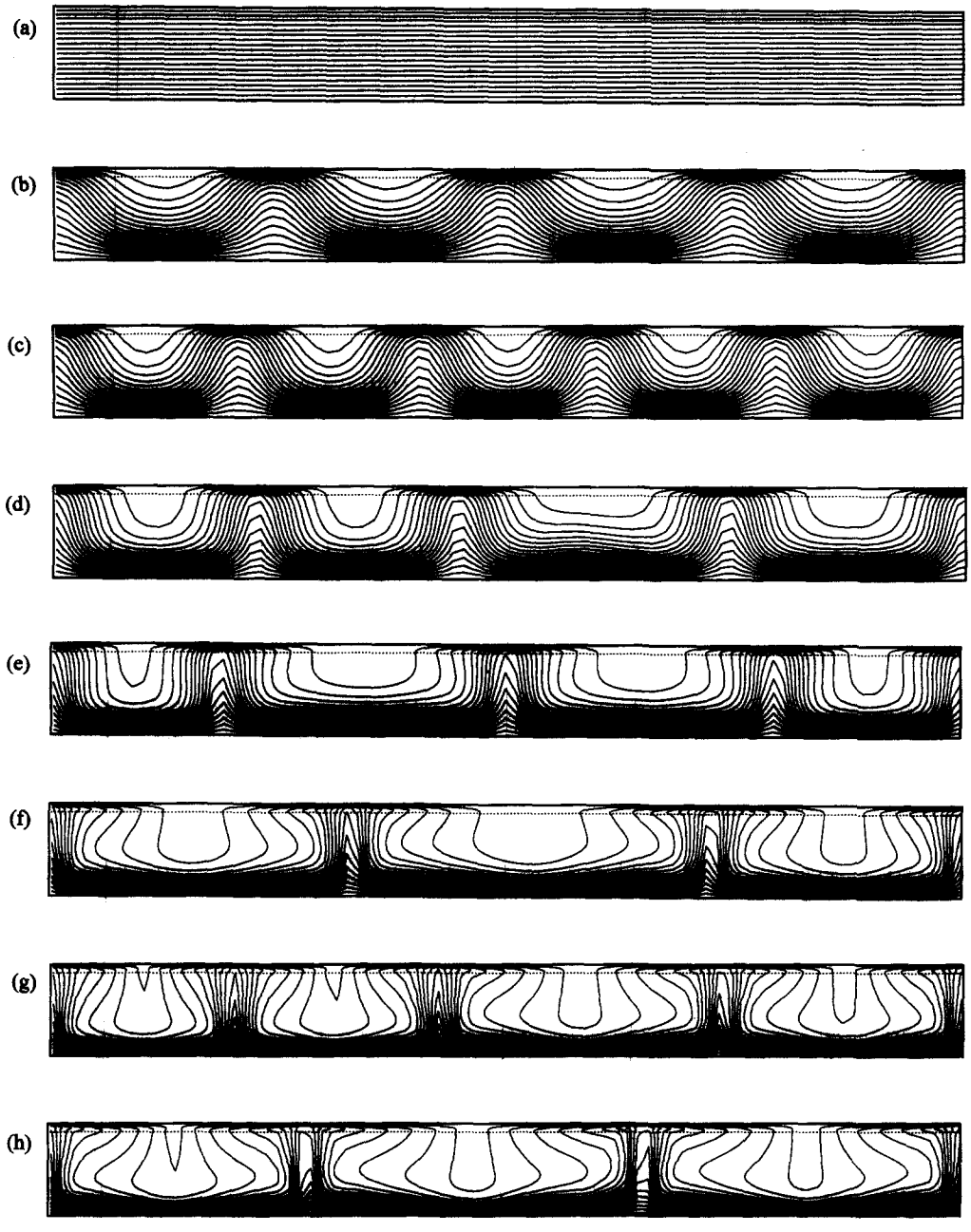

Fig. 8. Isotherms for $d = 0.1$ ($\Delta\theta = 0.05$ for all cases): (a) $Ra_p = Ra_{pc}$; (b) $Ra_p = 1.5Ra_{pc}$; (c) $Ra_p = 2Ra_{pc}$; (d) $Ra_p = 3Ra_{pc}$; (e) $Ra_p = 5Ra_{pc}$; (f) $Ra_p = 10Ra_{pc}$; (g) $Ra_p = 15Ra_{pc}$; (h) $Ra_p = 20Ra_{pc}$.

culating cells are continuously readjusting their positions and sizes in the iterative process for each case when $Ra_p \geqslant 3$ until the steady state is reached. Consequently, an excessive number of iterations were required to achieve an energy balance of less than 1%. Even after satisfying the convergence and energy balance criteria, some of the figures are not symmetrical, as shown in Figs. 7(d)–(h) and 8(d)–(h). To ensure that the streamlines and isotherms truly represent the final steady state results, at least 10 000 more iterations were performed for all cases when $Ra_p \geqslant 3$.

Figure 9 shows the corresponding Nusselt number, and the change in Nu is quite dramatic due to the change in the number of cells. It should be noted that whenever there is a reduction in the number of cells, the trend of the curve significantly changes. In particular, the Nusselt number remains nearly the same as Ra_p/Ra_{pc} increases from 7.5 to 10 due to the reduction in the number of cells from eight to six. When Ra_p/Ra_{pc} increases from 15 to 17.5, there is even a significant reduction in Nu. The Nusselt number computed by Chen and Chen [7] with the pre-determined wave-

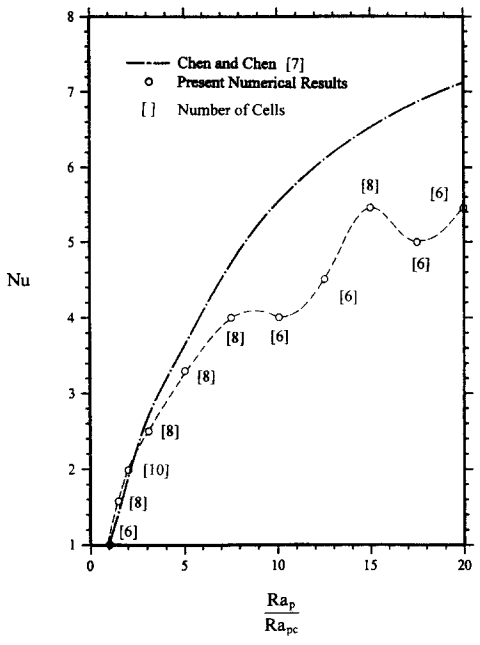

Fig. 9. Variation of the Nusselt number with the Rayleigh number for $d = 0.1$.

length is nearly the same as the present results only when $Ra_p/Ra_{pc} < 3$. On the other hand, their Nusselt number prediction may not be appropriate for the present aspect ratio and/or higher values of Ra_p/Ra_{pc}, although they successfully predicted the Nusselt number for $d = 1$ as explained earlier (see Fig. 4). It is worth mentioning that the change in Nu may not be as smooth as plotted in Fig. 9 because of the possible abrupt change in the number of cells with the increase of Ra_p/Ra_{pc}. Substantially more calculations are required to verify such a phenomenon.

In comparison with the experimental and numerical data [5, 7] as shown in Fig. 10, the present results slightly overpredict the Nusselt number at $Ra_p/Ra_{pc} = 1.25$, 1.5 and 1.75. However, the Nusselt number is nearly the same as their numerical data at $Ra_p/Ra_{pc} = 2.0$. Overall, the curve fit for the present

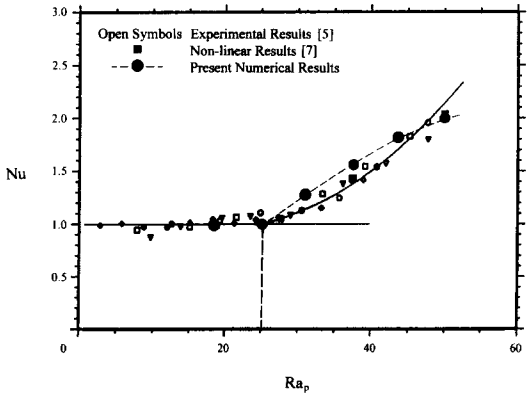

Fig. 10. Comparison of the present results of Nu with experimental and numerical data of Chen and Chen [7] when $d = 0.1$.

numerical data is upwardly convex in contrast to the previous investigators' [7] concave curve fit based on the experimental data for the given Ra_p range ($\leqslant 2$ Ra_{pc}). With the consideration of the numerical results by Chen and Chen [7], shown in Fig. 9, the upwardly convex curve fit seems appropriate. More experimental data points for the higher values of Ra_p are necessary to determine the rate of change in Nu in this range. It should be noted that the previous experimental report [5] clearly indicated that the flow pattern is three-dimensional. Although the present and previous [7] numerical calculations assumed two-dimensional convection rolls, the calculated Nusselt numbers are in good agreement with the experimental data. In general, the heat transfer rate in porous media computed by assuming two-dimensional rolls shows an excellent agreement with the experimental data in which the flow pattern is three-dimensional. Consequently, the Nusselt number in the supercritical region shown in Fig. 9 would be in good agreement with the experimental data. It will be very interesting to verify the present computational results in Nu and the number of cells experimentally for the range of the aspect ratio, $2 \leqslant Ra_p/Ra_{pc} \leqslant 20$.

Throughout the present study, the isotherms indicate that flow patterns in the fluid and porous layers are apparently in phase, as shown in Figs. 3 and 5. On the other hand, Chen and Chen [7] found that the flow patterns are out of phase since a weak plume descends in the porous region caused by the ascending plume in the fluid region. It is evident that they reported higher Nu numbers than those obtained by the present study in the supercritical range (Figs. 4 and 8) as discussed earlier. The higher heat transfer coefficients indicate more vigorously recirculating cells. Therefore, the flow patterns are out of phase because of the active momentum transfer along the interface. When the recirculating cells are less active, however, the isotherms are dominated by conduction. It should be noted that some of the flow patterns reported by Chen and Chen are also in phase (Figs. 7(a)–(c) [7]).

4. CONCLUSION

The buoyancy-induced convection when a porous layer underlying a fluid layer is heated from below has been numerically investigated. The numerical scheme used in the present study was found to predict the wavenumber accurately at the onset of convection compared with the linear stability theory. In addition, interesting and important results were observed at the supercritical Rayleigh number regime. When $d > 0.12$, the number of recirculating cells increases continuously as the Rayleigh number increases, which in turn increases the Nusselt number. For this depth ratio range, convection is limited to the fluid layer, while conduction is the dominating heat transfer mode in the porous layer.

For $d = 0.1$, however, the recirculating cells are

continuously readjusting their positions and sizes in the composite layer as the Rayleigh numbers increases. The number of cells in the supercritical convection regime does not increase monotonically. The corresponding Nusselt number variation is quite different from the previously reported numerical results with the pre-determined computational domain by the linear stability theory [7]. The present Nusselt number variation for $d = 0.1$ may not be smooth because of the possible abrupt change in the number of cells with the increase of the Rayleigh number in the supercritical region. This suggests the need for careful experimental work to identify the change in the Nusselt number with respect to the Rayleigh number for $d < 0.12$. Finally, it was verified that the present two-dimensional calculations predict reasonably well the heat transfer rate in the case of three-dimensional natural convection in the composite layer heated from below.

Acknowledgements—The authors wish to express their appreciation to Dr C. F. Chen, Professor of the Department of Aerospace and Mechanical Engineering at the University of Arizona, and Dr F. Chen, Associate Professor at National Taiwan University, for their valuable suggestions and discussions and for their help in providing us with the original figures during the preparation of this paper.

REFERENCES

1. V. Prasad, Convective flow interaction and heat transfer between fluid and porous layers. In *Convective Heat and Mass Transfer in Porous Media* (Edited by S. Kakac, B. Kilkis, F. A. Kulacki and F. Arinc), pp. 173–224. Kluwer Academic, Dordrecht (1991).
2. D. A. Nield and A. Bejan, *Convection in Porous Media*. Springer, New York (1992).
3. W. J. Sun, Convection instability in superposed porous and fluid layers, Ph.D. Dissertation, University of Minnesota, Minneapolis, MN (1973).
4. F. Chen and C. F. Chen, Onset of finger convection in a horizontal porous layer underlying a fluid layer, *J. Heat Transfer* **110,** 403–409 (1988).
5. F. Chen and C. F. Chen, Experimental investigation of convective stability in a superposed fluid and porous layer when heated from below, *J. Fluid Mech.* **207,** 311–321 (1989).
6. D. Poulikakos, Buoyancy-driven convection in a horizontal fluid layer extending over a porous substrate, *Physics Fluids* **29,** 3949–3957 (1986).
7. F. Chen and C. F. Chen, Convection in superposed fluid and porous layers, *J. Fluid Mech.* **234,** 97–119 (1992).
8. V. Prasad, K. Brown and Q. Tian, Flow visualization and heat transfer experiments in fluid-superposed porous layers heated from below, *Porous Media, Mixtures and Multiphase Heat Transfer, ASME HTD* **117,** 75–83 (1989).
9. V. Prasad and Q. Tian, An experimental study of thermal convection in fluid-superposed porous layers heated from below, *Proceedings of the Ninth International Heat Transfer Conference*, Vol. 5, pp. 207–212. Hemisphere, Washington, DC (1990).
10. K. Vafai and C. L. Tien, Boundary and inertia effects on flow and heat transfer in porous media, *Int. J. Heat Mass Transfer* **24,** 195–203 (1981).
11. M. Kaviany, *Principles of Heat Transfer in Porous Media*. Springer, New York (1991).
12. G. Neale and W. Nader, Practical significance of Brinkman extension of Darcy's law: coupled parallel flows within a channel and a boundary porous medium, *Can. J. Chem. Engng* **52,** 472–478 (1974).
13. K. Vafai and S. J. Kim, Analysis of surface enhancement by a porous substrate, *J. Heat Transfer* **112,** 700–706 (1990).
14. C. Beckermann, S. Ramadhyani and R. Viskanta, Natural convection flow and heat transfer between a fluid layer and a porous layer inside a rectangular enclosure, *J. Heat Transfer* **109,** 363–370 (1987).
15. S. Patankar, *Numerical Heat Transfer and Fluid Flow*. Hemisphere, New York (1980).
16. S. Nakamura, *Applied Numerical Methods with Software*. Prentice-Hall, New Jersey (1991).
17. S. Chandrasekhar, *Hydrodynamic and Hydromagnetic Stability*. Dover, New York (1991).
18. I. Catton, Effect of wall conduction on the stability of a fluid in a rectangular region heated from below, *J. Heat Transfer* **94,** 446–452 (1972).
19. I. Catton, The effect of insulating vertical walls on the onset of motion in a fluid heated from below, *Int. J. Heat Mass Transfer* **15,** 665–672 (1972).
20. P. Cheng, Geothermal heat transfer. In *Handbook of Heat Transfer Applications* (Edited by W. M. Rohsenow, J. P. Harnett and E. N. Garnic). McGraw-Hill, New York (1985).
21. D. Poulikakos, Thermal instability in a horizontal fluid layer superposed on a heat generating porous bed, *Numer. Heat Transfer* **12,** 83–99 (1987).